R-matrix calculation of antiproton capture by helium ions

Kazuhiro Sakimoto
Institute of Space and Astronautical Science, Japan Aerospace Exploration Agency, Yoshinodai, Sagamihara 229-8510, Japan
(Received 19 June 2007; published 24 October 2007)

Rigorous treatment is presented for antiproton capture by helium ions, i.e., $\bar{p}+\mathrm{He}^+ \rightarrow (\bar{p}\mathrm{He}^+)^{**} \rightarrow \bar{p}\mathrm{He}^{2+}+e$, by using *R*-matrix theory. The present work applies the *R*-matrix method to an exotic collision system containing an antiproton, a nucleus, and an electron. The eigenvalue problem in the *R*-matrix method is solved by the discrete-variable-representation algorithm without use of any decoupling approximation. The probability of antiproton capture is calculated for the total angular momentum $J=30$. A huge number of the overlapping resonances are found to be prominent everywhere over a wide range of energies. As suggested in a time-dependent wave-packet propagation calculation [K. Sakimoto, Phys. Rev. A **74**, 022709 (2006)], the resonances make a dominant contribution to the antiproton capture. It is found that the nonadiabatic coupling is always weak in off-resonance collisions, but can be very strong in resonance collisions.

DOI: 10.1103/PhysRevA.76.042513 PACS number(s): 36.10.−k, 34.50.Lf, 34.80.Lx

I. INTRODUCTION

Recently, considerable attention has been paid to *antiprotonic helium* $\bar{p}\mathrm{He}^+$ [1]. The $\bar{p}\mathrm{He}^+$ atoms are produced when antiprotons $\bar{p}$ are stopped in liquid or gaseous helium. The $\bar{p}\mathrm{He}^+$ formation is considered to account for the existence of long-lived $\bar{p}$ against annihilation or nuclear absorption [2,3]. Actually, the produced $\bar{p}\mathrm{He}^+$ atoms are always in the metastable states embedded in electron continuum, and decay by means of Auger transitions [1–3]. Some of them have very long Auger lifetime ($\gg 1$ ps), and could be directly observed in high-resolution laser spectroscopic experiments [1]. Several sophisticated calculations have been also carried out for the metastable states of $\bar{p}\mathrm{He}^+$ [4–8]. The spectroscopic studies of $\bar{p}\mathrm{He}^+$ are now very important for the determination of the fundamental physical quantities such as antiproton mass [1,9,10].

As a collision process, the importance of the metastable states (i.e., resonances) has been pointed out for the $\bar{p}$ capture in $\bar{p}+\mathrm{He}^+$ [11] (in what follows referred to as paper I), i.e.,

$$\bar{p}+\mathrm{He}^+ \rightarrow \bar{p}\mathrm{He}^{2+}+e \rightarrow (\bar{p}\mathrm{He}^+)^{**} \rightarrow \bar{p}\mathrm{He}^{2+}+e. \quad (1)$$

The attractive Coulomb interaction, working not only between the reactants ($\bar{p}$ and He^+) but also between the products (e and $\bar{p}\mathrm{He}^{2+}$), can yield a great abundance of resonances in this collision system. In paper I, however the detailed structure of the resonances could not be resolved, and the examination was given only for the resonance-averaged quantities. This is because the calculation was based on the time-dependent wave-packet propagation method, which was unsuitable for the case that the collision energy was low and the interaction was strong attraction.

For the investigation of the resonance phenomena, the *R*-matrix method [12] is very famous, and has been applied to a wide variety of problems [13]. The essential idea of this method is that we divide the configuration space into two regions by setting a boundary in the relative distance of the incident particle and the target: in the inner region, the solution of the bound-state problem is used to obtain the logarithmic derivative of the scattering wave function on the boundary; and connecting the wave function to the outer region, we can calculate the scattering *S* matrix. In particular, one-time-only diagonalization in the inner region can provide scattering information over a wide range of energies.

In this study, we present rigorous *R*-matrix treatment for the $\bar{p}+\mathrm{He}^+$ collisions. The eigenvalues and eigenvectors in the *R*-matrix method are accurately calculated by direct numerical solution based on discrete variable representation (DVR) [14–17]. So far, the application of the *R*-matrix method to heavy particle collisions is rare in atomic and molecular physics [18–22]. The heavy particle collisions participate in molecular dissociation by electron impacts as an exit channel. The *R*-matrix calculation, mostly based on the fixed-nuclei or fixed-nuclear rotation approximation [23], has been carried out for this problem [24–26]. The present calculation is free from any type of decoupling approximation.

The investigation of the present exotic system involves treating several interesting problems well known in atomic and molecular physics. The antiprotonic helium ion $\bar{p}\mathrm{He}^{2+}$ is a hydrogenic atom, and hence the states having the same principal quantum number are degenerate in the nonrelativistic approximation. Furthermore, this ion can be regarded as a typical dipole. The $\bar{p}\mathrm{He}^{2+}$ atom was detected in a recent experimental study [27], and is now a practical subject of research in atomic physics. In a different perspective, the $\bar{p}\mathrm{He}^+$ can be rather assumed to be a molecule [1,28]. To clarify to what extent the Born-Oppenheimer (BO) separation of the e and $\bar{p}\mathrm{He}^{2+}$ motions is applicable is a very intriguing subject [28]. The inverse process of (1) may be associated with *dissociative recombination* (DR) in electron-molecule scattering. The DR occurs through a nonadiabatic process, and further depends strongly on the resonance phenomena. Enormous challenges are still continuing for the understanding of the DR mechanism [29]. Because it is completely feasible to do a detailed calculation for the three-body problem, the present exotic system can be a model case for the study of the reaction dynamics involving both the electron and nucleus motions.

In the present study, the range of the total energy E considered is $-2<E<-1.8$ a.u., which is much lower than the first excited-state ($2s$ or $2p$) energy (−0.5 a.u.) of the He^+

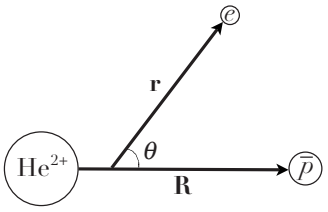

FIG. 1. Jacobi coordinates of the present system.

ion. Therefore, only the ground $(1s)$ state of He^+ is open as the asymptotic $\bar{p}+He^+$ channel. [The rest energy of the separation limit $\bar{p}+He^+(1s)$ is $E=-2$ a.u.] We focus on an overall picture of the capture process over the present energy range, and accordingly broad resonances are rather important. Due to a large amount of computational labor, the calculation is carried out only for the total angular momentum $J=30$. However, this is sufficient for the understanding of the importance of the resonance phenomena in the $\bar{p}$ capture process. (Antiprotons are trapped into orbits having an angular momentum of typically $\lesssim 30$ at low energies [11].) In previous studies, of special interest were the metastable $\bar{p}He^+$ states with a circular or near-circular orbit [1–10,28]. At the present energies, these circular-state resonances take place only if $J\sim 38$, and usually have a very narrow width. Furthermore, the $\bar{p}$ capture itself becomes insignificant for $J \gtrsim 38$ [11]. The partial waves $J\sim 38$ are not a typical case of the $\bar{p}$ capture collisions in the present energy region.

II. COLLISION THEORY

A. Schrödinger equation

As shown in Fig. 1, we use the Jacobi coordinates $(\mathbf{r},\mathbf{R})$ corresponding to the $e+\bar{p}He^{2+}$ arrangement. Then, we can write the total Hamiltonian as

$$\tilde{H} = -\frac{1}{2m_r}\frac{\partial^2}{\partial r^2}r + \frac{\tilde{\mathbf{l}}^2}{2m_r r^2} - \frac{1}{2m_R}\frac{\partial^2}{\partial R^2}R + \frac{\tilde{\mathbf{L}}^2}{2m_R R^2} + V, \tag{2}$$

where the reduced masses are given by

$$m_r = \frac{m_e(m_{\bar{p}}+m_{\mathrm{He}^{2+}})}{m_e+m_{\bar{p}}+m_{\mathrm{He}^{2+}}}, \quad m_R = \frac{m_{\bar{p}}m_{\mathrm{He}^{2+}}}{m_{\bar{p}}+m_{\mathrm{He}^{2+}}}, \tag{3}$$

with $m_e(=1)$ being the electron mass, $m_{\bar{p}}$ the antiproton mass, and $m_{\mathrm{He}^{2+}}$ the helium nucleus (alpha particle) mass. In (2), $\tilde{\mathbf{l}}$ is the electronic angular-momentum vector (operator), and $\tilde{\mathbf{L}}$ is the angular-momentum vector of $\bar{p}$-He^{2+}. The interaction $V=V(r,R,\theta)$ is given by

$$V = -\frac{2}{|(m_R/m_{\mathrm{He}^{2+}})\mathbf{R}+\mathbf{r}|} + \frac{1}{|(m_R/m_{\bar{p}})\mathbf{R}-\mathbf{r}|} - \frac{2}{R}, \tag{4}$$

and is expressed as a function of r, R, and the angle θ between $\mathbf{r}$ and $\mathbf{R}$. Here and in the following, we use atomic units unless otherwise stated. The nonrelativistic approximation is assumed, all the particles are considered to be pointlike, and the spin of the particles is omitted for simplicity.

The time-independent Schrödinger equation for the present system at the total energy E is

$$\tilde{H}\Psi^{JMp}_{\tau_0}(\mathbf{r},\mathbf{R}) = E\Psi^{JMp}_{\tau_0}(\mathbf{r},\mathbf{R}), \tag{5}$$

where (J,M) are the total angular-momentum quantum numbers, p is the total parity, and τ_0 indicates the initial channel.

B. $e+\bar{p}He^{2+}$ channel

First, we consider the product channel $e+\bar{p}He^{2+}$ in the reaction (1). As usually done, the total wave function $\Psi^{JMp}_{\tau_0}(\mathbf{r},\mathbf{R})$ can be expanded as

$$\Psi^{JMp}_{\tau_0}(\mathbf{r},\mathbf{R}) = (rR)^{-1}\sum_{NL\ell}\mathcal{Y}^{JMp}_{L\ell}(\hat{\mathbf{r}},\hat{\mathbf{R}})\Upsilon_{NL}(R)f^{Jp}_{NL\ell,\tau_0}(r), \tag{6}$$

where the angular part is

$$\mathcal{Y}^{JMp}_{L\ell}(\hat{\mathbf{r}},\hat{\mathbf{R}}) = \sum_m (LM-m,\ell m|JM)Y_{LM-m}(\hat{\mathbf{R}})Y_{\ell m}(\hat{\mathbf{r}}) \tag{7}$$

with $Y_{LM-m}(\hat{\mathbf{R}})$ and $Y_{\ell m}(\hat{\mathbf{r}})$ being the spherical harmonics, $(LM-m,\ell m|JM)$ the Clebsch-Gordan coefficient [30], and ℓ the electronic angular-momentum quantum number. The function $\Upsilon_{NL}(R)$, with (N,L) being the principal and angular-momentum quantum numbers, represents the bound state of the hydrogenic ion $\bar{p}He^{2+}$. The total parity p is specifically given by $p=(-1)^{L+\ell}$.

We define a radial distance r_0 such that the interaction can be assumed to be $V=-1/r-2/R$ and the contribution from closed channels is negligible at $r>r_0$. Then, the radial function $f^{Jp}_{NL\ell,\tau_0}(r)$ at $r>r_0$ for the open channel (N,L,ℓ) can be expressed in terms of the Coulomb functions $s(\epsilon,\ell;r)$ and $c(\epsilon,\ell;r)$, i.e.,

$$f^{Jp}_{NL\ell,\tau_0}(r) = s(\epsilon,\ell;r)\delta_{NL\ell,\tau_0} + c(\epsilon,\ell;r)\mathcal{K}^{Jp}_{NL\ell,\tau_0}, \tag{8}$$

where $\mathcal{K}^{Jp}_{NL\ell,\tau_0}$ is the scattering K-matrix element. The functions $s(\epsilon,\ell;r)$ and $c(\epsilon,\ell;r)$ have the asymptotic forms [31]:

$$s(\epsilon,\ell;r) \sim \left(\frac{m_r}{2\pi k_N}\right)^{1/2}\sin(\xi), \tag{9}$$

$$c(\epsilon,\ell;r) \sim \left(\frac{m_r}{2\pi k_N}\right)^{1/2}\cos(\xi), \tag{10}$$

where

$$\xi = k_N r - \frac{\ell\pi}{2} + \frac{m_r}{k_N}\ln(2k_N r) + \arg\Gamma\left(\ell+1-i\frac{m_r}{k_N}\right), \tag{11}$$

$$\epsilon = E - E_N = \frac{k_N^2}{2m_r}, \tag{12}$$

with $E_N=-2m_R/N^2$ being the energy of the $\bar{p}He^{2+}$ ion.

C. $\bar{p}+He^+$ channel

For the description of the $\bar{p}+He^+$ reactants, paper I has shown that the adiabatic basis in the BO separation is very

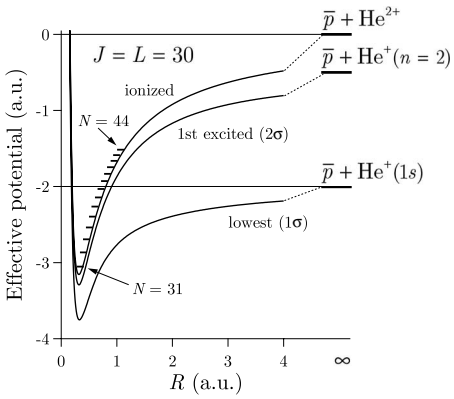

FIG. 2. Effective (adiabatic) potentials of the $\bar{p}$+He$^+$ and $\bar{p}$ +He^{2+} systems for J=L=30. The $\bar{p}$He^{2+} energy levels E_N (N =31,32,…,44) are also plotted.

useful. This allows us to employ the Jacobi coordinates $(\mathbf{r},\mathbf{R})$ also for the asymptotic $\bar{p}$+He$^+$ channel. We introduce a body-fixed (BF) frame in which the z axis is chosen along $\mathbf{R}$. The rotation from a space-fixed (SF) frame to the BF frame is represented by the Euler angles (α,β,γ), where the first two angles are equal to $\hat{\mathbf{R}}=(\beta,\alpha)$ in the SF frame, and a rotation γ about the z axis is made such that $\mathbf{r}$ lies in the xz plane. In the BF frame, the operator $\tilde{\mathbf{L}}^2$ in (2) should read as [32]

$$\tilde{\mathbf{L}}^2 = (\tilde{\mathbf{J}} - \tilde{\mathbf{l}})^2 = \tilde{\mathbf{J}}^2 + \tilde{\mathbf{l}}^2 - 2\tilde{J}_z\tilde{l}_z - \tilde{l}_+\tilde{J}_- - \tilde{l}_-\tilde{J}_+, \tag{13}$$

where $\tilde{\mathbf{J}}$ is the total angular-momentum vector.

Because of the total energies $E \ll -0.5$ a.u., it is sufficient to consider only the lowest adiabatic (i.e., 1σ) state as the reactant channel. For each fixed R, the 1σ adiabatic potential energy $E_{1\sigma}(R)$ is calculated by the equation

$$\tilde{H}_{\mathrm{BO}}\frac{\chi_{1\sigma}(R;r,\theta)}{r} = E_{1\sigma}(R)\frac{\chi_{1\sigma}(R;r,\theta)}{r}, \tag{14}$$

where

$$\tilde{H}_{\mathrm{BO}} = -\frac{1}{2m_r}\frac{\partial^2}{\partial r^2}r + \frac{\tilde{\mathbf{l}}^2}{2m_r r^2} + V, \tag{15}$$

and the adiabatic wave function $\chi_{1\sigma}(R;r,\theta)$ is normalized to unity. Figure 2 shows the effective potentials, $J(J+1)/2m_R R^2 + E_{n\sigma}(R)$ $(n=1,2)$ for $\bar{p}$+He$^+$ and $L(L+1)/2m_R R^2 - 2/R$ for $\bar{p}$+He^{2+}. In the adiabatic picture, the channels of electronic excitation and ionization become locally open only for $R \lesssim 1$ a.u. if $E \lesssim -1.8$ a.u.

We define a radial distance R_0 ($\sim$1 a.u.) such that the nonadiabatic coupling is negligible at $R > R_0$. Then, the total wave function $\Psi^{JMp}_{\tau_0}(\mathbf{r},\mathbf{R})$ at $R > R_0$ has the BO separation form [11,33]

$$\Psi^{JMp}_{\tau_0}(\mathbf{r},\mathbf{R}) = (rR)^{-1}\mathcal{D}^{Jp}_{M0}(\alpha,\beta,\gamma)\chi_{1\sigma}(R;r,\theta)F^{Jp}_{1\sigma,\tau_0}(R), \tag{16}$$

where

$$\mathcal{D}^{Jp}_{M\lambda}(\alpha,\beta,\gamma) = \left(\frac{2J+1}{16\pi^2(1+\delta_{\lambda,0})}\right)^{1/2}[D^J_{M\lambda}(\alpha,\beta,\gamma) + p(-1)^{J+\lambda}D^J_{M,-\lambda}(\alpha,\beta,\gamma)]^* \tag{17}$$

with $D^J_{M\lambda}(\alpha,\beta,\gamma)$ being the Wigner's rotation matrix element [30], and $\lambda = \tilde{J}_z = \tilde{l}_z$ the magnetic quantum number in the BF frame.

The scattering radial function $F^{Jp}_{1\sigma,\tau_0}(R)$ can be expressed in terms of the WKB functions [11,33], i.e.,

$$F^{Jp}_{1\sigma,\tau_0}(R) = S(E,J;R)\delta_{1\sigma,\tau_0} + C(E,J;R)\mathcal{K}^{Jp}_{1\sigma,\tau_0}, \tag{18}$$

$$S(E,J;R) = \left(\frac{m_R}{2\pi K_{1\sigma}(R)}\right)^{1/2}\sin(\Xi), \tag{19}$$

$$C(E,J;R) = \left(\frac{m_R}{2\pi K_{1\sigma}(R)}\right)^{1/2}\cos(\Xi), \tag{20}$$

where

$$\Xi = \int^R K_{1\sigma}(R')dR', \tag{21}$$

$$K_{1\sigma}(R) = \left[2m_R\left(E - \frac{(J+1/2)^2}{2m_R R^2} - E_{1\sigma}(R)\right)\right]^{1/2}. \tag{22}$$

D. Antiproton capture

Because the Coulomb potential range is longer than the centrifugal one (cf. Fig. 2), even in the limit of zero collision energy, the product $\bar{p}$He^{2+} can have a wide range of angular momenta $0 \le L \lesssim 38$ [11]. Furthermore, the ejected electron cannot carry off large kinetic energy. Therefore, we can expect that the antiproton is mainly captured into very high (N,L) orbits. In the reaction process (1), although only a single channel is open for the reactants, we have a large number of open channels for the products.

The S-matrix element $(\mathbb{S})_{\tau,\tau'} = \mathcal{S}^{Jp}_{\tau,\tau'}$, with $\tau,\tau' = 1\sigma$ or (N,L,ℓ), is defined by the matrix equation

$$\mathbb{S} = (1+i\mathbb{K})(1-i\mathbb{K})^{-1}, \tag{23}$$

where $\mathbb{K}_{\tau,\tau'} = \mathcal{K}^{Jp}_{\tau,\tau'}$. Then, the total probability of the $\bar{p}$ capture (1) can be given by

$$P^{Jp} = \sum_{NL\ell}|\mathcal{S}^{Jp}_{NL\ell,1\sigma}|^2. \tag{24}$$

The probability of the capture into the (N,L) state is

$$P^{Jp}(NL) = \sum_{\ell}|\mathcal{S}^{Jp}_{NL\ell,1\sigma}|^2. \tag{25}$$

The angular momentum (ℓ) distribution of the ejected electron is

$$P^{Jp}(\ell) = \sum_{NL}|\mathcal{S}^{Jp}_{NL\ell,1\sigma}|^2. \tag{26}$$

The cross section for the capture is given by

$$\sigma = \frac{\pi\Omega}{2m_R E_{\rm col}}, \tag{27}$$

where $E_{\rm col}=E-E_{1\sigma}(\infty)$ is the center-of-mass collision energy of $\bar{p}+\mathrm{He}^+$, and

$$\Omega = \sum_{Jp} (2J+1)P^{Jp} \tag{28}$$

is the collision strength defined in paper I. Due to the peculiarity of the attractive Coulomb interaction, the collision strength does not vanish in the limit as $E_{\rm col}\to 0$, and correspondingly the cross section diverges as $(E_{\rm col})^{-1}$ [11].

III. *R*-MATRIX METHOD

A. Inner region

In the R-matrix theory using the nonuniform boundary condition, we consider the following eigenvalue problem [17,24]:

$$(\tilde{H}+\tilde{\mathcal{L}}_r+\tilde{\mathcal{L}}_R)\Phi_\rho^{JMp}(\mathbf{r},\mathbf{R}) = E_\rho \Phi_\rho^{JMp}(\mathbf{r},\mathbf{R}). \tag{29}$$

The Bloch operators $\tilde{\mathcal{L}}_r$ and $\tilde{\mathcal{L}}_R$ are given by [34]

$$\tilde{\mathcal{L}}_r = \frac{1}{2m_r a}\delta(r-a)\frac{\partial}{\partial r}r, \tag{30}$$

$$\tilde{\mathcal{L}}_R = \frac{1}{2m_R A}\delta(R-A)\frac{\partial}{\partial R}R, \tag{31}$$

where $r=a$ and $R=A$ are the boundaries defining the inner region, and are chosen such that $\mathrm{Y}_{NL}(R)=0$ at $R\geq A$ for all the relevant channels (N,L) and $\chi_{1\sigma}(R;r,\theta)=0$ at $r\geq a$ for $R\sim A$ (see Fig. 3). The wave function $\Phi_\rho^{JMp}(\mathbf{r},\mathbf{R})$ can be normalized to unity, i.e.,

$$\langle \Phi_\rho^{JMp} | \Phi_{\rho'}^{JMp}\rangle_{a,A} = \delta_{\rho,\rho'}, \tag{32}$$

where the subscript a,A indicates that the range of the integral is limited to the inner region of $0\leq r\leq a$ and $0\leq R\leq A$.

If the radial distance r is close to the boundary a, the wave function Φ_ρ^{JMp} in the inner region can be expanded suitably in the form corresponding to the $e+\bar{p}\mathrm{He}^{2+}$ arrangement (cf. Sec. II B),

$$\Phi_\rho^{JMp}(\mathbf{r},\mathbf{R}) = (rR)^{-1}\sum_{NL\ell}\mathcal{Y}_{L\ell}^{JMp}(\hat{\mathbf{r}},\hat{\mathbf{R}})\mathrm{Y}_{NL}(R)h_{NL\ell,\rho}^{Jp}(r). \tag{33}$$

Furthermore, if $R\sim A>R_0$, corresponding to the $\bar{p}+\mathrm{He}^+$ arrangement, the wave function Φ_ρ^{JMp} can be expressed as (cf. Sec. II C)

$$\Phi_\rho^{JMp}(\mathbf{r},\mathbf{R}) = (rR)^{-1}\mathcal{D}_{M0}^{Jp}(\alpha,\beta,\gamma)\chi_{1\sigma}(R;r,\theta)H_{1\sigma,\rho}^{Jp}(R). \tag{34}$$

Within the inner region, we can always expand the scattering wave function $\Psi_{\tau_0}^{JMp}(\mathbf{r},\mathbf{R})$ in terms of the R-matrix wave function $\Phi_\rho^{JMp}(\mathbf{r},\mathbf{R})$ [12], i.e.,

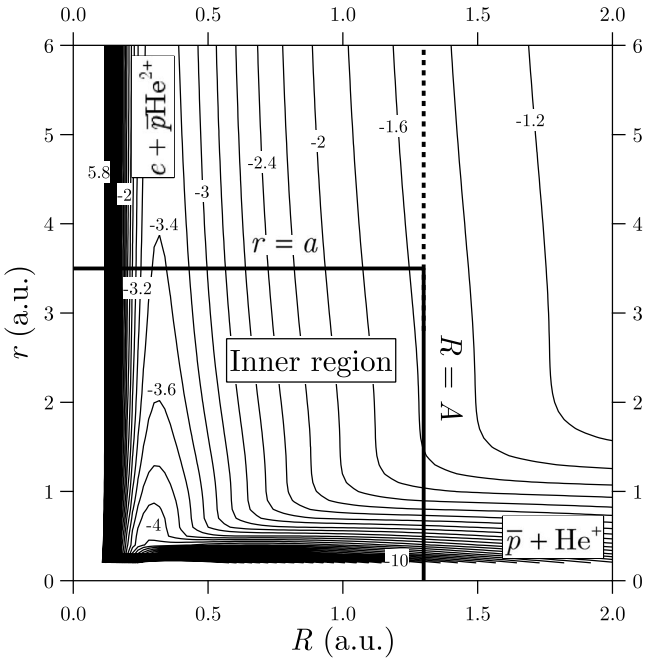

FIG. 3. Contour plots of the interaction $J(J+1)/(2m_R R^2)+V(r,R,\theta)$ at $\theta=\pi/4$ for $J=30$. The boundary of the inner region is indicated by the bold lines. The range of the total energies treated in the present calculation is $E<-1.8$ a.u.

$$\Psi_{\tau_0}^{JMp}(\mathbf{r},\mathbf{R}) = \sum_\rho X_{\tau_0,\rho}^{Jp}\Phi_\rho^{JMp}(\mathbf{r},\mathbf{R}). \tag{35}$$

To determine the expansion coefficient $X_{\tau_0,\rho}^{Jp}$, we consider the relation

$$\begin{aligned}\langle \Phi_\rho^{JMp}|\tilde{H}+\tilde{\mathcal{L}}_r+\tilde{\mathcal{L}}_R-E|\Psi_{\tau_0}^{JMp}\rangle_{a,A} &= \langle \Phi_\rho^{JMp}|\tilde{\mathcal{L}}_r+\tilde{\mathcal{L}}_R|\Psi_{\tau_0}^{JMp}\rangle_{a,A} \\ &= (E_\rho-E)\langle \Phi_\rho^{JMp}|\Psi_{\tau_0}^{JMp}\rangle_{a,A}.\end{aligned} \tag{36}$$

Using (6), (16), (33), and (34), we can show that the coefficient $X_{\tau_0,\rho}^{Jp}$ is given by

$$\begin{aligned}X_{\tau_0,\rho}^{Jp} = &\frac{1}{2m_r(E_\rho-E)}\sum_{NL\ell}h_{NL\ell,\rho}^{Jp}(a)\frac{df_{NL\ell,\tau_0}^{Jp}}{dr}(a) \\ &+\frac{1}{2m_R(E_\rho-E)}H_{1\sigma,\rho}^{Jp}(A)\frac{dF_{1\sigma,\tau_0}^{Jp}}{dR}(A).\end{aligned} \tag{37}$$

Then, we have from (35) and (37),

$$\begin{aligned}f_{NL\ell,\tau_0}^{Jp}(a) = &\sum_{N'L'\ell'}\mathcal{R}_{NL\ell,N'L'\ell'}^{Jp}\frac{df_{N'L'\ell',\tau_0}^{Jp}}{dr}(a) \\ &+\mathcal{R}_{NL\ell,1\sigma}^{Jp}\frac{dF_{1\sigma,\tau_0}^{Jp}}{dR}(A)\end{aligned} \tag{38}$$

and

$$F^{Jp}_{1\sigma,\tau_0}(A) = \mathcal{R}^{Jp}_{1\sigma,1\sigma}\frac{dF^{Jp}_{1\sigma,\tau_0}}{dR}(A) + \sum_{N'L'\ell'} \mathcal{R}^{Jp}_{1\sigma,N'L'\ell'}\frac{df^{Jp}_{N'L'\ell',\tau_0}}{dr}(a), \quad (39)$$

where the *R*-matrix elements [12,24] are defined by

$$\mathcal{R}^{Jp}_{NL\ell,N'L'\ell'} = \frac{1}{2m_r}\sum_\rho \frac{h^{Jp}_{NL\ell,\rho}(a)h^{Jp}_{N'L'\ell',\rho}(a)}{E_\rho - E}, \quad (40)$$

$$\mathcal{R}^{Jp}_{1\sigma,1\sigma} = \frac{1}{2m_R}\sum_\rho \frac{[H^{Jp}_{1\sigma,\rho}(A)]^2}{E_\rho - E}, \quad (41)$$

$$m_R\mathcal{R}^{Jp}_{NL\ell,1\sigma} = m_r\mathcal{R}^{Jp}_{1\sigma,NL\ell} = \frac{1}{2}\sum_\rho \frac{h^{Jp}_{NL\ell,\rho}(a)H^{Jp}_{1\sigma,\rho}(A)}{E_\rho - E}. \quad (42)$$

B. Body-fixed frame

To solve the eigenvalue problem (29), we adopt the same BF frame as introduced in Sec. II C. In the BF frame, the *R*-matrix wave function Φ^{JMp}_ρ in the inner region can be accurately expanded as [35]

$$\Phi^{JMp}_\rho = (rR)^{-1}\sum_\lambda \mathcal{D}^{Jp}_{M\lambda}(\alpha,\beta,\gamma)\phi^{Jp\lambda}_\rho(r,R,\theta). \quad (43)$$

Differently from the description of the asymptotic $\bar{p}+\mathrm{He}^+$ channel (Sec. II C), the magnetic quantum numbers λ are coupled in the inner region, and no adiabatic basis functions are introduced in this expansion. It follows from (17) that the summation in (43) is taken for $\lambda \geq 0$ if $p=(-1)^J$ and for $\lambda \geq 1$ if $p=(-1)^{J+1}$. Because the asymptotic $\bar{p}+\mathrm{He}^+$ channel is the σ state, only the parity $p=(-1)^J=(-1)^{L+\ell}$ is allowed in the $\bar{p}$ capture (1). Inserting the expansion (43) into (29), we have the eigenvalue equation in the form

$$\begin{aligned}
&\sum_{\lambda'}[\tilde{M}^{Jp}_{\lambda,\lambda'} + V(r,R,\theta)]\phi^{Jp\lambda'}_\rho(r,R,\theta) \\
&= \left[\frac{1}{2m_r}\left(-\frac{\partial^2}{\partial r^2} + \delta(r-a)\frac{\partial}{\partial r}\right)\right. \\
&\quad \left. + \frac{1}{2m_R}\left(-\frac{\partial^2}{\partial R^2} + \delta(R-A)\frac{\partial}{\partial R}\right)\right]\phi^{Jp\lambda}_\rho(r,R,\theta) \\
&\quad + \left(\frac{\tilde{\mathbf{l}}^2}{2m_r r^2} + \frac{J(J+1) - \tilde{\mathbf{l}}^2 - 2\lambda^2}{2m_R R^2} + V(r,R,\theta)\right) \\
&\quad \times \phi^{Jp\lambda}_\rho(r,R,\theta) - \frac{1}{2m_R R^2}(1+\delta_{\lambda,0})^{1/2}[J(J+1) \\
&\quad - \lambda(\lambda+1)]^{1/2}\left(-\frac{\partial}{\partial\theta} - (\lambda+1)\cot\theta\right)\phi^{Jp\lambda+1}_\rho(r,R,\theta) \\
&\quad - \frac{1}{2m_R R^2}(1+\delta_{\lambda,1})^{1/2}[J(J+1) - \lambda(\lambda-1)]^{1/2} \\
&\quad \times \left(\frac{\partial}{\partial\theta} - (\lambda-1)\cot\theta\right)\phi^{Jp\lambda-1}_\rho(r,R,\theta) \\
&= E_\rho\phi^{Jp\lambda}_\rho(r,R,\theta). \quad (44)
\end{aligned}$$

The BF wave function $\phi^{Jp\lambda}_\rho(r,R,\theta)$ satisfies

$$\sum_\lambda \langle\phi^{Jp\lambda}_\rho|\phi^{Jp\lambda}_{\rho'}\rangle_{a,A} = \delta_{\rho,\rho'}. \quad (45)$$

The SF and BF angular functions are related by [35]

$$\mathcal{Y}^{JMp}_{L\ell}(\hat{\mathbf{r}},\hat{\mathbf{R}}) = \sum_\lambda U^{Jp\ell}_{L\lambda}\mathcal{D}^{Jp}_{M\lambda}(\alpha,\beta,\gamma)\mathcal{P}^\lambda_\ell(\cos\theta), \quad (46)$$

where $\mathcal{P}^\lambda_\ell(\cos\theta) = \sqrt{2\pi}Y_{\ell\lambda}(\theta,0)$ is the associated Legendre function normalized to unity, and

$$U^{Jp\ell}_{L\lambda} = \left(\frac{2L+1}{2J+1}\right)^{1/2}(L0,\ell\lambda|J\lambda)\frac{1+p(-1)^{L+\ell}}{[2(1+\delta_{\lambda,0})]^{1/2}} \quad (47)$$

is the SF-BF frame transformation matrix element. Using (46), we can easily show that the amplitude of the SF radial function $h^{Jp}_{NL\ell,\rho}(r)$ at $r=a$ is

$$h^{Jp}_{NL\ell,\rho}(a) = \sum_\lambda U^{Jp\ell}_{L\lambda}\langle\mathcal{P}^\lambda_\ell\mathrm{Y}_{NL}|\phi^{Jp\lambda}_\rho\rangle|_{r=a}. \quad (48)$$

Actually in the numerical calculation of the eigenvalue equation (44), the quantum numbers λ larger than some value $\lambda_{\max}$ are excluded. To ensure consistency of the numbers of the SF and BF basis sets, we should consider the electronic angular momenta $\ell \leq \lambda_{\max}$. Using (34), we have for the amplitude of the BF radial function $H^{Jp}_{1\sigma,\rho}(R)$ at $R=A$,

$$H^{Jp}_{1\sigma,\rho}(A) = \langle\chi_{1\sigma}|\phi^{Jp\lambda=0}_\rho\rangle|_{R=A}. \quad (49)$$

Equations (48) and (49) are used to evaluate the *R*-matrix elements (40)–(42).

C. Outer propagation for $e+\bar{p}\mathrm{He}^{2+}$

For the reduction of the numerical labor, it is preferable to make the inner region as small as possible. However, because of the long-range dipole interaction working between *e* and $\bar{p}\mathrm{He}^{2+}$ and the degeneracy of the $\bar{p}\mathrm{He}^{2+}$ hydrogenic sublevels associated with high *N* states, we need a very large value of r_0 to assume the scattering asymptotic form (8) in the $e+\bar{p}\mathrm{He}^{2+}$ channel. Dubau introduced the proper regular and irregular functions including the dipole-coupling effect in place of $s(\epsilon,\ell;r)$ and $c(\epsilon,\ell;r)$ in (8) [36]. In the present calculation, we resolve the problem by propagating the *R* matrix to a sufficiently large distance $r=a_n$. We can follow the idea of Stechel *et al.* [37] and of Baluja *et al.* [38]. For the $\bar{p}+\mathrm{He}^+$ channel, which can be nicely described by the 1σ adiabatic state, such labor is unnecessary.

We divide the configuration space enclosed by $a \leq r \leq a_n$ and $0 \leq R \leq A$ into *n* blocks each defined by $a_{\kappa-1} \leq r \leq a_\kappa$ ($\kappa=1,\ldots,n$), where $a_0=a$. The outermost boundary a_n is taken to be $a_n > r_0$. We diagonalize the Hermitian operator $\tilde{H}+\tilde{\mathcal{L}}_{\mathrm{out}}$ in the block region of $a_{\kappa-1} \leq r \leq a_\kappa$, i.e.,

$$(\tilde{H}+\tilde{\mathcal{L}}_{\rm out})\bar{\Phi}_\rho^{JMp}(\mathbf{r},\mathbf{R})=\bar{E}_\rho\bar{\Phi}_\rho^{JMp}(\mathbf{r},\mathbf{R}), \tag{50}$$

where the Bloch operator is given by

$$\tilde{\mathcal{L}}_{\rm out}=\frac{1}{2m_r a_\kappa}\delta(r-a_\kappa)\frac{\partial}{\partial r}r-\frac{1}{2m_r a_{\kappa-1}}\delta(r-a_{\kappa-1})\frac{\partial}{\partial r}r, \tag{51}$$

and $\bar{E}_\rho$ is the eigenvalue. We write the R matrix defined at $r=a_\kappa$ in the matrix form

$$\mathbb{R}(a_\kappa)=\begin{bmatrix}\mathbb{R}_{\bar{p}\bar{p}}(a_\kappa) & \mathbb{R}_{\bar{p}e}(a_\kappa)\\ \mathbb{R}_{e\bar{p}}(a_\kappa) & \mathbb{R}_{ee}(a_\kappa)\end{bmatrix}, \tag{52}$$

where "e" denotes the $e+\bar{p}\mathrm{He}^{2+}$ channel and "$\bar{p}$" denotes the $\bar{p}+\mathrm{He}$ channel. Then, we can show that the R matrix is propagated by the following scheme:

$$\mathbb{R}_{ee}(a_\kappa)=\mathbb{T}_{11}-\mathbb{T}_{10}[\mathbb{R}_{ee}(a_{\kappa-1})+\mathbb{T}_{00}]^{-1}\mathbb{T}_{01}, \tag{53}$$

$$\mathbb{R}_{e\bar{p}}(a_\kappa)=\mathbb{T}_{10}[\mathbb{R}_{ee}(a_{\kappa-1})+\mathbb{T}_{00}]^{-1}\mathbb{R}_{e\bar{p}}(a_{\kappa-1}), \tag{54}$$

$$\mathbb{R}_{\bar{p}\bar{p}}(a_\kappa)=\mathbb{R}_{\bar{p}\bar{p}}(a_{\kappa-1})-\mathbb{R}_{\bar{p}e}(a_{\kappa-1})[\mathbb{R}_{ee}(a_{\kappa-1})+\mathbb{T}_{00}]^{-1}\mathbb{R}_{e\bar{p}}(a_{\kappa-1}), \tag{55}$$

$$\mathbb{R}_{\bar{p}e}(a_\kappa)=\mathbb{R}_{\bar{p}e}(a_{\kappa-1})[\mathbb{R}_{ee}(a_{\kappa-1})+\mathbb{T}_{00}]^{-1}\mathbb{T}_{01}, \tag{56}$$

where $\mathbb{T}_{\eta\eta'}$ $(\eta,\eta'=0,1)$ is given by [38]

$$(\mathbb{T}_{\eta\eta'})_{N\ell,N'L'\ell'}=\frac{1}{2m_r}\sum_\rho\frac{\bar{h}^{Jp}_{N\ell,\rho}(a_{\kappa+\eta-1})\bar{h}^{Jp}_{N'L'\ell',\rho}(a_{\kappa+\eta'-1})}{\bar{E}_\rho-E}. \tag{57}$$

The radial function $\bar{h}^{Jp}_{N\ell,\rho}(r)$ in the block region is defined just in the same way as (33).

D. Scattering boundary condition

The K matrix is calculated from the R matrix evaluated at $r=a_n$ by [39]

$$\mathbb{K}=-(\mathbf{c}-\mathbb{R}_{\rm oo}\mathbf{\hat{c}})^{-1}(\mathbf{s}-\mathbb{R}_{\rm oo}\mathbf{\hat{s}}), \tag{58}$$

where we have set

$$(\mathbf{s})_{1\sigma,\tau}=S(E,J;A)\delta_{1\sigma,\tau}, \tag{59}$$

$$(\mathbf{s})_{\tau,\tau'}=s(\epsilon,\ell;a_n)\delta_{\tau,\tau'}\quad \text{for}\quad \tau\neq 1\sigma, \tag{60}$$

$$(\mathbf{c})_{1\sigma,\tau}=C(E,J;A)\delta_{1\sigma,\tau}, \tag{61}$$

$$(\mathbf{c})_{\tau,\tau'}=c(\epsilon,\ell;a_n)\delta_{\tau,\tau'}\quad \text{for}\quad \tau\neq 1\sigma, \tag{62}$$

and $\mathbb{R}_{\rm oo}$ is the open-channel part of the R-matrix $\mathbb{R}(a_n)$.

IV. R-MATRIX CALCULATION

A. Numerical solution

To perform the numerical calculation of the R-matrix eigenvalue problem (44), we use the DVR algorithm [14–17], in which the grid of points (r_i,R_j,θ_k) in the configuration space is constructed from the zero points of orthogonal polynomials, and the wave function $\phi_\rho^{Jp\lambda}$ is directly evaluated at these grid points. The applicability of the DVR method to the R-matrix calculation was discussed in several studies [17,40–42].

In the DVR method, by taking a linear combination of orthogonal polynomials $Q_\nu(x)$ normalized to unity, we define grid-based functions for each coordinate in the form

$$u_\mu(x)=[\omega_\mu W(x)]^{1/2}\sum_\nu^{N_x}Q_\nu(x)Q_\nu(x_\mu)=\frac{[W(x)]^{1/2}Q_{N_x}(x)}{\omega_\mu^{1/2}(x-x_\mu)\dot{Q}_{N_x}(x_\mu)}, \tag{63}$$

where x_μ $(\mu=1,2,\ldots,N_x)$ are the zero points of $Q_{N_x}(x)$, ω_μ is the quadrature weight, $W(x)$ is the weight function, and $\dot{Q}_{N_x}=dQ_{N_x}/dx$. The grid-based functions (63) satisfy the following orthogonal properties:

$$u_\mu(x_{\mu'})=\left(\frac{W_\mu}{\omega_\mu}\right)^{1/2}\delta_{\mu,\mu'},\quad (u_\mu|u_{\mu'})=\delta_{\mu,\mu'}, \tag{64}$$

where we have set $W_\mu=W(x_\mu)$, and the integral is made over the range of x. Then, we may expand the R-matrix wave function $\phi_\rho^{Jp\lambda}$ in (43) as

$$\phi_\rho^{Jp\lambda}(r,R,\theta)=\sum_{ijk}^{N_rN_RN_\theta}\left(\frac{\omega_i\omega_j\omega_k}{W_iW_jW_k}\right)^{1/2}\phi_\rho^{Jp\lambda}(r_i,R_j,\theta_k)u_i(r)\times u_j(R)u_k(\theta), \tag{65}$$

and we have simultaneous linear equations with respect to the values of the wave function given at the grid points, i.e.,

$$\sum_{\lambda'i'j'k'}[M^{Jp}_{\lambda ijk,\lambda'i'j'k'}+V(r_i,R_j,\theta_k)\delta_{\lambda ijk,\lambda'i'j'k'}]\phi^{Jp\lambda'}_{\rho,i'j'k'}=E_\rho\phi^{Jp\lambda}_{\rho,ijk}, \tag{66}$$

where we have defined

$$\phi^{Jp\lambda}_{\rho,ijk}=\left(\frac{\omega_i\omega_j\omega_k}{W_iW_jW_k}\right)^{1/2}\phi_\rho^{Jp\lambda}(r_i,R_j,\theta_k) \tag{67}$$

and

$$M^{Jp}_{\lambda ijk,\lambda'i'j'k'}=(u_iu_ju_k|\tilde{M}^{Jp}_{\lambda,\lambda'}|u_{i'}u_{j'}u_{k'}). \tag{68}$$

For the outer propagation of the R matrix, computer codes are available in the CPC library [38,43]. However, because the present program code for the inner region can be easily rewritten for the outer region, we employ the DVR solution also for the eigenvalue problem of $\tilde{H}+\tilde{\mathcal{L}}_{\rm out}$. We express the wave function $\bar{\Phi}_\rho^{JMp}$ in each outer block as

$$\bar{\Phi}_\rho^{JMp}=(rR)^{-1}\sum_\lambda\mathcal{D}^{Jp}_{M\lambda}(\alpha,\beta,\gamma)\bar{\phi}_\rho^{Jp\lambda}(r,R,\theta), \tag{69}$$

where again we assume

$$\bar{\phi}_{\rho}^{Jp\lambda}(r,R,\theta)=\sum_{ijk}^{\bar{N}_r\bar{N}_R\bar{N}_\theta}\left(\frac{\bar{\omega}_i\bar{\omega}_j\bar{\omega}_k}{\bar{W}_i\bar{W}_j\bar{W}_k}\right)^{1/2}\bar{\phi}_{\rho}^{Jp\lambda}(\bar{r}_i,\bar{R}_j,\bar{\theta}_k)\bar{u}_i(r)\times\bar{u}_j(R)\bar{u}_k(\theta), \quad (70)$$

with $\bar{u}_i(r)$, $\bar{u}_j(R)$, and $\bar{u}_k(\theta)$ being the grid-based functions defined in the outer block. The unknown quantities $\bar{\phi}_{\rho}^{Jp\lambda}(\bar{r}_i,\bar{R}_j,\bar{\theta}_k)$ are determined in the same way as the inner-region solution.

B. Choice of orthogonal polynomials

For the diagonalization of the operator $\tilde{H}+\tilde{\mathcal{L}}_r+\tilde{\mathcal{L}}_R$, the grid-based functions are required to have unfixed values of logarithmic derivatives at $r=a$ or $R=A$. The application of the nonuniform boundary condition is essential for an efficient *R*-matrix calculation [17]. For this purpose, Baye *et al.* [17] introduced Jacobi polynomials $P_{\nu}^{(\alpha,\beta)}(x)$ with $\alpha=0$, $\beta=2$ [44]. Using the Jacobi polynomials, we have the grid-based functions for the coordinate r as

$$u_i(r)=\frac{[\omega_i W(r)]^{1/2}}{a^3}\sum_{\nu=0}^{N_r}(2\nu+3)P_{\nu}^{(0,2)}(x)P_{\nu}^{(0,2)}(x_i t), \quad (71)$$

with $W(r)=r^2$ and $x=(2r-a)/a$. The functions $u_i(r)$ satisfy the physical boundary condition

$$u_i(0)=0. \quad (72)$$

Due to the introduction of the Bloch operator $\tilde{\mathcal{L}}_r$ and the boundary condition (72), the matrix elements are certainly symmetric, i.e.,

$$\left\langle u_i\left|-\frac{d^2}{dr^2}+\delta(r-a)\frac{d}{dr}\right|u_{i'}\right\rangle=-\langle u_i|\ddot{u}_{i'}\rangle_a+u_i(a)\dot{u}_{i'}(a)=\langle\dot{u}_i|\dot{u}_{i'}\rangle_a, \quad (73)$$

where $\dot{u}_i=du_i/dr$ and $\ddot{u}_i=d^2u_i/dr^2$. The explicit form of the matrix elements are given by Baye *et al.* [17]. For the coordinate R, the gird-based functions $u_j(R)$ with $0\le R\le A$ are defined exactly in the same way as (71). For the remaining coordinate θ, as discussed in Refs. [33,45], we can use Legendre polynomials $P_{\nu}(\cos\theta)$ if λ=even, and ultraspherical polynomials $P_{\nu}^{(1,1)}(\cos\theta)$ [44] if λ=odd.

Some other types of orthogonal polynomials having unfixed logarithmic derivatives on the boundary were examined in Refs. [17,41,42]. If we wish to impose the zero derivative on the boundary, the second kind of Chebyshev polynomials $\sin[(2\nu-1)\pi x/2]$ are appropriate. The corresponding grid-based functions automatically satisfy $u_i(0)=0$ and $\dot{u}_i(a)=0$. This is just the same as employed by Layton [40]. In this case, however we need to introduce the Buttle correction [46], which is crucial for accuracy improvement in the *R*-matrix calculation [12,13,17,40].

For the diagonalization of the operator $\tilde{H}+\tilde{\mathcal{L}}_{\rm out}$, as done by Baluja *et al.* [38], we can adopt Legendre polynomials defined in the range of $a_{\kappa-1}\le r\le a_{\kappa}$, i.e.,

$$\bar{u}_i(r)=\frac{\bar{\omega}_i^{1/2}}{a_\kappa-a_{\kappa-1}}\sum_{\nu=0}^{\bar{N}_r}(2\nu+1)P_{\nu}(x)P_{\nu}(x_i), \quad (74)$$

with

$$x=\frac{2}{a_\kappa-a_{\kappa-1}}\left(r-\frac{a_{\kappa-1}+a_\kappa}{2}\right). \quad (75)$$

The use of the functions (74) allows us to have arbitrary logarithmic derivatives at $r=a_{\kappa-1}$ and a_κ. For the coordinates R and θ, we have used the same grid-based functions as for the inner region, i.e., $\bar{u}_j(R)=u_j(R)$ and $\bar{u}_k(\theta)=u_k(\theta)$.

C. Calculation

We solve the eigenvalue problems for $\tilde{H}+\tilde{\mathcal{L}}_r+\tilde{\mathcal{L}}_R$ and $\tilde{H}+\tilde{\mathcal{L}}_{\rm out}$, and then save the eigenvalues E_ρ and $\bar{E}_{\bar{\rho}}$, and the amplitudes $h_{NL\ell,\rho}^{Jp}(a)$, $H_{1\sigma,\rho}^{Jp}(A)$, $\bar{h}_{NL\ell,\bar{\rho}}^{Jp}(a_{\kappa-1})$, and $\bar{h}_{NL\ell,\bar{\rho}}^{Jp}(a_\kappa)$ in a storage device. These quantities are obtained independently of the total (or collision) energy. The calculation for the inner region is the most time-consuming part of the computation. However, once these data are stored, the collision calculation at any energy can be accomplished by a sequence of simple operations: the construction of the inner *R* matrix (40)–(42), the outer propagation of the *R* matrix (53)–(56), and the construction of the *K* matrix (58). In the present study, the calculation was carried out for $(J,p)=(30,0)$.

Relevant values of the numerical parameters, a, A, N_r, N_R, N_θ, $\lambda_{\max}$, and $a_1,\ldots,a_n$ are to be determined prior to the main calculation. Paper I suggested that if $A>1$ a.u., the scattering boundary condition (18) could be applied (e.g., Fig. 2). Indeed, the present choice $A=1.3$ a.u. was found to give capture probabilities within the error of $<2\%$. We chose $a=a_0=3.5$ a.u. and $a_\kappa=40\kappa$ a.u. $(\kappa=1,2,\ldots,n)$. Because the interaction becomes weak at $r>a$, and the kinetic energy of ejected electrons is small, $\bar{N}_r=20$ is sufficient for the outer propagation. The positional relationship of the boundaries a and A in the interaction contour map can be viewed in Fig. 3.

The convergence properties of the capture probability with respect to N_r, N_R, and N_θ are summarized in Fig. 4 for a specific resonance. In the following, we carried out the calculation by choosing $N_r=30$, $N_R=60$, and $N_\theta=5$. Large $\lambda_{\max}$ would be required if we discussed some very narrow resonances [5]. In the present study, however we focus on broad resonances, and as done in paper I, the $\lambda=0$ and 1 states were coupled.

V. COLLISION CALCULATION

To find the appropriate outermost boundary a_n, we calculated the total capture probabilities P^{Jp} for three different values of $a_n=40$, 120, and 200 a.u. At energies $-1.990\le E\le-1.965$ a.u., as shown in the upper panel of Fig. 5, the smallest value $a_n=40$ turns out to be practically sufficient. However, the collision calculation using $a_n=40$ a.u. cannot produce any resonances at energies $-1.945\le E\le1.936$ a.u. (the lower panel of Fig. 5). The resonances appearing at these energies are composed of a high Rydberg electronic

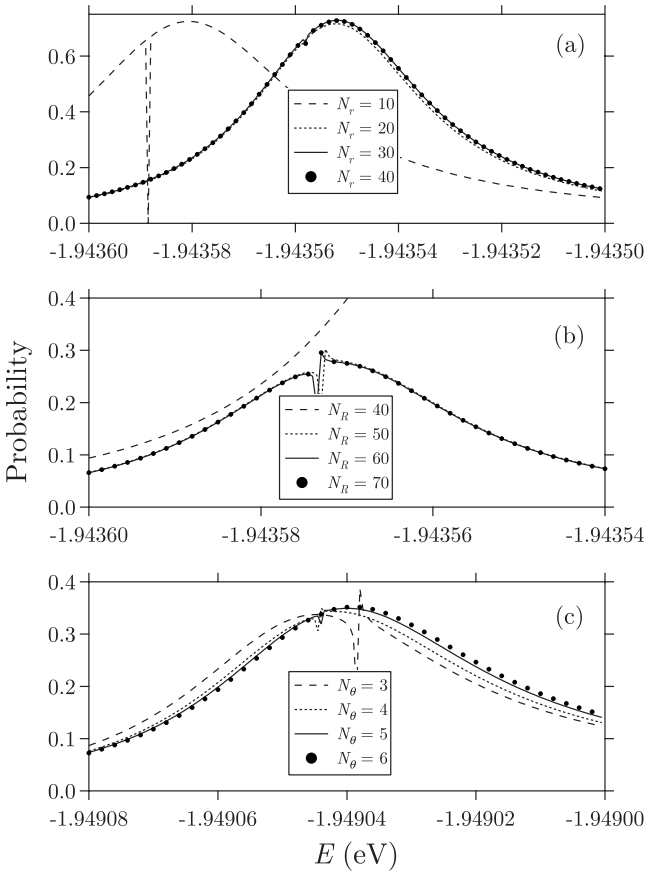

FIG. 4. Convergence properties of the total capture probability P^{Jp} for $J=30$. The boundaries are set to $a=a_n=3.5$ a.u. and $A=1.3$ a.u. (a) N_r dependence for $N_R=40$, $N_\theta=3$, and $\lambda_{\max}=0$. (b) N_R dependence for $N_r=30$, $N_\theta=3$, and $\lambda_{\max}=0$. (c) N_θ dependence for $N_r=20$, $N_R=50$, and $\lambda_{\max}=1$.

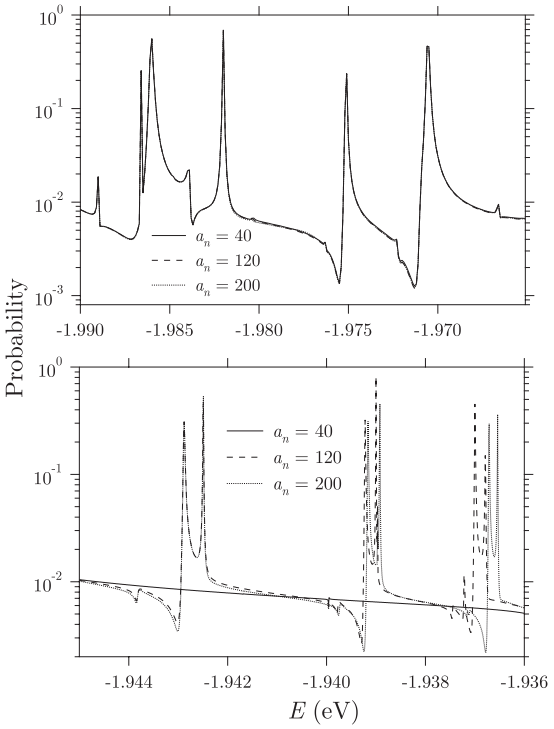

FIG. 5. Total capture probabilities P^{Jp} for $J=30$ at total energies of $-1.990 \leq E \leq -1.965$ a.u. and $-1.945 \leq E \leq 1.936$ a.u., calculated by choosing $a_n=40$, 120, and 200 a.u.

state, and thereby the effect of the dipole interaction must be taken into account more carefully. Although such high Rydberg resonances are observed only in a limited energy range, we choose $a_n=200$ a.u. for all the calculations shown later.

In Fig. 6, we show the total capture probabilities P^{Jp} at total energies ranging from $E=-2$ a.u. up to $E=-1.80$ a.u. (i.e., at collision energies $0<E_{\rm col}\leq 5.442$ eV), by setting mostly $\Delta E=10^{-4}$ a.u. as the interval for the energy scan. As was expected in paper I, the $\bar{p}$ capture probability exhibits a quite complicated structure due to overlapping resonances. We show in the figure the positions of the $\bar{p}{\rm He}^{2+}$ energies $E_{N=39}=-1.9289$ a.u. and $E_{N=40}=-1.8336$ a.u. At energies just below $E=E_N$, resonances appear in a Rydberg series converging to E_N, as could be already seen in the lower panel of Fig. 5. (Very high Rydberg resonances are not shown in Fig. 6 because the outermost boundary a_n should be taken larger than the present value for those resonances.)

In Fig. 6, we also show the positions of some bound (vibrational) energy levels supported by the 2σ and 1π adiabatic potential curves. The number attached to the right-hand side of the symbol 2σ or 1π in the figure is defined by $N_{\rm res}=v+L_{\rm res}+1$, where $L_{\rm res}$ is the rotational quantum number of the vibrational bound state, and v is the vibrational quantum number. If the energy is very low, i.e., $E\lesssim -3$ a.u., it was found in previous studies that the adiabatic approximation was appropriate for the description of the (1σ) resonance states [1,5,28]. In Fig. 6, the resonance just above the $(2\sigma,41)$ levels and the one just above $(2\sigma,42)$ seem to have a similar profile, and hence may be both assigned to the 2σ state. However, any resonance cannot be easily identified as

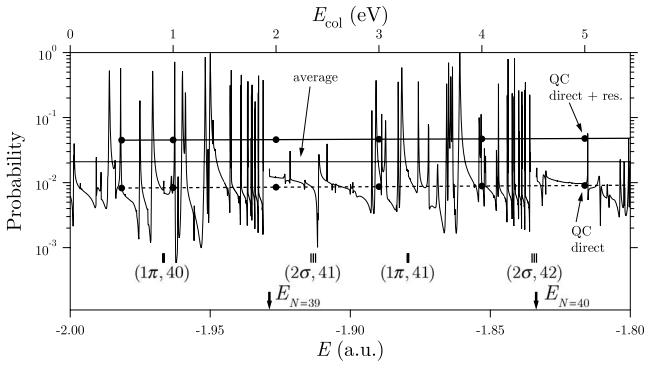

FIG. 6. Total capture probabilities P^{Jp} for $J=30$ as a function of the total energy E (or the collision energy $E_{\rm col}$). The interval for the energy scan is $\Delta E=10^{-4}$ or 10^{-5} a.u. The vertical lines with an arrow indicate the $\bar{p}{\rm He}^{2+}$ energies E_N for $N=39$ and 40. The other vertical lines indicate the energy levels supported by the 2σ and 1π effective adiabatic potential curves with the angular momenta of $L_{\rm res}=29$, 30, and 31. The assignment number $N_{\rm res}=40-42$ is given by $N_{\rm res}=v+L_{\rm res}+1$, with v being the vibrational quantum number. The horizontal line indicates the average probability $P^{Jp}_{\rm av}$. The results $P^{Jp}_{\rm dir}$ and $P^{Jp}_{\rm tot}=P^{Jp}_{\rm dir}+P^{Jp}_{\rm res}$ calculated by using the QC method [11] are also shown.

the 1π levels. Paper I suggested that the nonadiabatic coupling became important for resonance states. The assignment of the resonances by the adiabatic states would be effective only for the lowest 1σ and possibly 2σ. If the energy is just below $E=E_N$, the resonances forming a Rydberg series would be analyzed properly by using quantum-defect theory [47,48]. The correct understanding of the resonance phenomena associated with intermediate adiabatic states $(1\pi,\ 3\sigma,\ \ldots)$ requires an accurate calculation such as the present one.

In paper I, it has been found that the quantum-classical (QC) hybrid method, in which the electron motion is described by quantum mechanics and the heavy particle motion by classical mechanics, is very useful for our estimating the probability of the direct (off-resonance) $\bar{p}$ capture ($P_{\rm dir}^{Jp}$) and the resonance-averaged probability of the $\bar{p}$ capture into resonance states ($P_{\rm res}^{Jp}$). Figure 6 also shows the probabilities $P_{\rm dir}^{Jp}$ and $P_{\rm tot}^{Jp}=P_{\rm dir}^{Jp}+P_{\rm res}^{Jp}$ obtained by the QC calculation. Indeed, the QC probability $P_{\rm dir}^{Jp}$ seems to be regarded as the background direct contribution in the present *R*-matrix result. We also show the average probability defined by

$$P_{\rm av}^{Jp}=(E_{\rm max}-E_{\rm min})^{-1}\int_{E_{\rm min}}^{E_{\rm max}}P^{Jp}dE, \tag{76}$$

where $E_{\rm min}=-2.00$ a.u. and $E_{\rm max}=-1.80$ a.u. We can see that the probability $P_{\rm av}^{Jp}$ is much larger than the QC result $P_{\rm dir}^{Jp}$. This directly confirms the conjecture of paper I that the resonance process dominates the $\bar{p}$ capture in (1). The fact that $P_{\rm tot}^{Jp}$ is larger than $P_{\rm av}^{Jp}$ is taken as a matter of course because the resonance state can decay into either of $e+\bar{p}{\rm He}^{2+}$ or $\bar{p}+{\rm He}^{+}$. By using the present and QC results, we can estimate the (resonance-averaged) branching ratio of the $e+\bar{p}{\rm He}^{2+}$ decay as $(P_{\rm av}^{Jp}-P_{\rm dir}^{Jp})/P_{\rm res}^{Jp}=0.325$. Then, assuming that the branching ratio is independent of E and J, and using the fitting form of the cross section found in paper I, we can obtain the resonance-averaged capture cross section approximated to

$$\sigma\ ({\rm a.u.})=\frac{1.45}{E_{\rm col}\ ({\rm eV})} \tag{77}$$

if $E_{\rm col}<10$ eV. It should be remembered that the averaging over resonances becomes of no meaning at low energies. In the limit as $E_{\rm col}\to 0$, the $(E_{\rm col})^{-1}$ dependence of the cross section is strictly valid [11] although the determination of the constant term requires a detailed calculation for every partial wave J.

The partial capture probabilities $P^{Jp}(\ell)$, $P^{Jp}(NL)$, and $P^{Jp}(L)=\Sigma_N P^{Jp}(NL)$ are shown at energies of $-1.987\le E\le -1.968$ a.u. in Fig. 7. We can see that both the structure and the magnitude of $P^{Jp}(\ell=0)$ are very similar to those of $P^{Jp}(L=30)$. This reflects the angular-momentum conservation. In the case of $\ell=1$, the two values of $L=29$ and 31 are allowed. Actually, the fact that $P^{Jp}(L=29)$ is much larger than $P^{Jp}(L=31)$ indicates that the lower angular-momentum state is preferably occupied in the $\bar{p}$ capture.

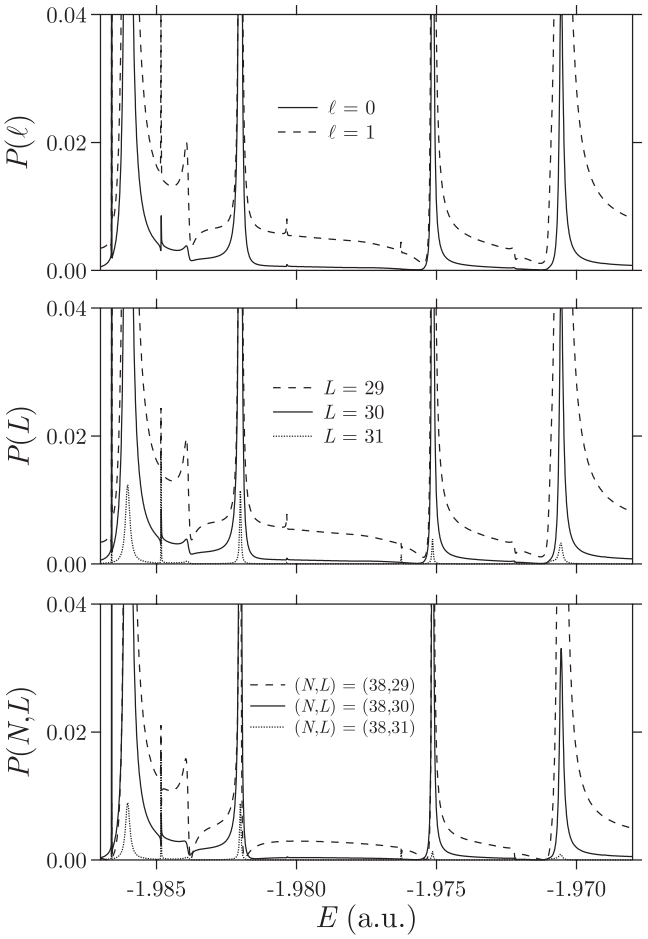

FIG. 7. Partial capture probabilities $P^{Jp}(\ell)$, $P^{Jp}(L)=\Sigma_N P^{Jp}(NL)$, and $P^{Jp}(NL)$ for $J=30$ at total energies of $-1.987\le E\le -1.968$ a.u. The interval for the energy scan is $\Delta E=10^{-5}$ a.u.

The N distribution $P^{Jp}(N)=\Sigma_L P^{Jp}(NL)$ is shown in Fig. 8 for three different energy regions of $-1.987\le E\le -1.968$ a.u. (region I), $-1.892\le E\le -1.880$ a.u. (region II), and $-1.812\le E\le -1.801$ a.u. (region III). The maximum value of the open channels N is $N_{\rm max}=38$ in region I, $N_{\rm max}=39$ in region II, and $N_{\rm max}=40$ in region III. We can see that the probability $P^{Jp}(N)$ becomes the largest mostly for $N=N_{\rm max}$. This means that the ejected electron tends to carry off the kinetic energy as small as possible. This N distribution differs from that estimated from the energy-matching condition [1]: in the latter case, the most occupied state should be invariably $N=\sqrt{m_R}\simeq 38$. It should be mentioned that the present argument is given for the partial wave $J=30$. However, we can find the trend of slow electron escape also by observing the $\bar{p}$ capture cross sections in $\bar{p}+{\rm H}$ collisions [49,50]. We can expect that the trend in the N distribution found for $J=30$ is seen generally for other J's in the present system.

VI. SUMMARY AND DISCUSSION

An accurate *R*-matrix calculation was carried out for $\bar{p}+{\rm He}^{+}$ collisions by using the DVR numerical algorithm. The

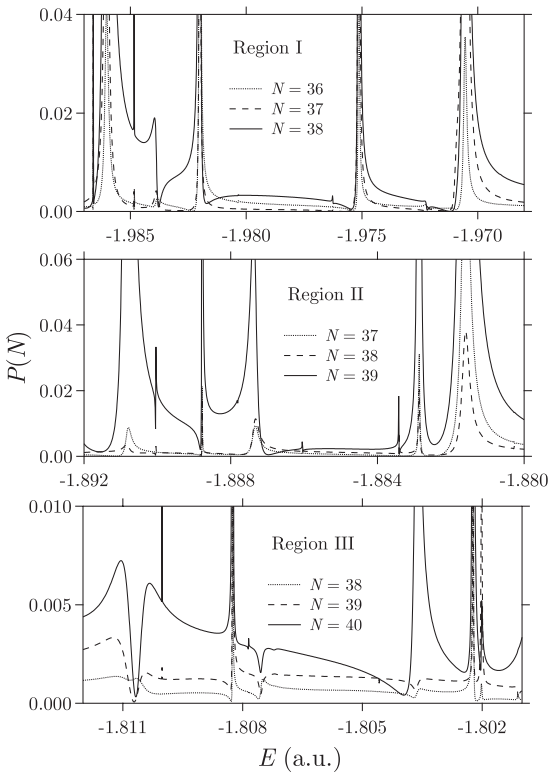

FIG. 8. Partial capture probabilities $P^{Jp}(N)=\Sigma_L P^{Jp}(NL)$ for $J=30$ at total energies of $-1.987 \leq E \leq -1.968$ a.u. (region I), $-1.892 \leq E \leq -1.880$ a.u. (region II), and $-1.812 \leq E \leq -1.801$ a.u. (region III). The interval for the energy scan is $\Delta E = 10^{-5}$ a.u.

present system is characterized by strong attractive interaction and rich resonances. The *R*-matrix method works most powerfully in such a case. Because of the long-range dipole interaction and the degeneracy of high-lying hydrogenic $\bar{p}He^{2+}$ states, the *R* matrix must be propagated to a very long distance for the $e+\bar{p}He^{2+}$ channel. This is especially important if a resonance is formed in a high Rydberg electronic state.

By the present *R*-matrix calculation, we can directly confirm the finding of paper I that the resonances make a dominant contribution to the $\bar{p}$ capture. At low collision energies, the $\bar{p}$ capture probability may be considered to provide a measure of the breakdown of the BO separation (i.e., the importance of the nonadiabatic coupling) in the $\bar{p}+He^+$ system. The off-resonance capture probability is very small <0.01, and the resonance-averaged capture probability is still small ~ 0.02. These results seem to support the validity of the BO separation. However, if the collision satisfies a resonance condition, the capture probability can be large (>0.1) and even close to unity (Fig. 6). Furthermore, the resonances are very rich everywhere. Thus, the situation for the applicability of the BO separation to the $\bar{p}+He^+$ collisions is complicated. The richness of the resonances would be the reason that the capture cross section in $\bar{p}+He^+$ is considerably overestimated by the Fermion molecular dynamics method [51], which is based on a classical-trajectory calculation. It is evident that the classical-trajectory treatment can never take account of the resonance effect. Generally in the collisions between an antiproton and an atomic ion, we may expect that the nonadiabatic coupling can be very strong if the resonance condition is satisfied. In the low-energy $\bar{p}$ capture by complex atomic ions, multielectron ejection may promptly occur just at some resonance energies.

The *R*-matrix calculation of the inner region is extremely laborious. For the calculation of the capture cross section, it is strongly desired at this time that some appropriate approximation can be introduced. One such candidate is the fixed-nuclear rotation (i.e., λ-conserving) approximation [23,52]. However, this approximation would be invalid in the outer region ($r \gg a$) because the coupling due to the long-range dipole interaction is still non-negligible, and the electrons escape slowly. Considering that the calculation of the outer region is not so troublesome, it is a good idea that the fixed-nuclear rotation approximation is applied to only the inner-region calculation. The study using such a hybrid method is now in progress, and will be reported in the near future.

Using the local-complex-potential model, which is constructed to reproduce the high-energy quantum-mechanical results, the present author has indicated that several resonances can be observed in the $\bar{p}$ capture by H atoms at very low collision energies <0.1 eV [53]. These are classified as a shape resonance predicted by the $\bar{p}+H$ adiabatic potential curve. Furthermore, the $\bar{p}p$ atom (i.e., *protonium*), as a dipole system, can bind an electron [54,55]. This suggests the possibility of the existence of another resonance phenomenon in $\bar{p}+H$ collisions [56]. Although the resonances may not be so prominent as those in the present case, it is very interesting to investigate whether such resonances really occur in the $\bar{p}+H$ system. Also for this purpose, the *R*-matrix method will be promising.

ACKNOWLEDGMENTS

The author would like to thank Professor I. Shimamura for valuable advice and comments. The present work was partially supported by the Grant-in-Aid for Scientific Research from the Ministry of Education, Science, Sports, and Technology of Japan.

[1] T. Yamazaki *et al.*, Phys. Rep. **366**, 183 (2002).
[2] G. T. Condo, Phys. Lett. **9**, 65 (1964).
[3] J. E. Russell, Phys. Rev. Lett. **23**, 63 (1969).
[4] N. Elander and E. Yarevsky, Phys. Rev. A **56**, 1855 (1997).
[5] V. I. Korobov and I. Shimamura, Phys. Rev. A **56**, 4587 (1997).
[6] J. Révai and A. T. Kruppa, Phys. Rev. A **57**, 174 (1998).
[7] O. I. Kartavtsev, D. E. Monakhov, and S. I. Fedotov, Phys.

Rev. A **61**, 062507 (2000).
[8] Y. Kino, M. Kamimura, and H. Kudo, Nucl. Instrum. Methods Phys. Res. B **214**, 84 (2004).
[9] M. Hori *et al.*, Phys. Rev. Lett. **91**, 123401 (2003).
[10] M. Hori *et al.*, Phys. Rev. Lett. **96**, 243401 (2006).
[11] K. Sakimoto, Phys. Rev. A **74**, 022709 (2006) (referred to as paper I).
[12] P. G. Burke and W. D. Robb, Adv. At. Mol. Phys. **11**, 143 (1975).
[13] P. G. Burke and K. A. Berrington, *Atomic and Molecular Processes: An R-Matrix Approach* (Institute of Physics, Bristol, Philadelphia, 1993).
[14] J. C. Light, I. P. Hamilton, and J. V. Lill, J. Chem. Phys. **82**, 1400 (1985).
[15] F. Calogero, J. Math. Phys. **22**, 919 (1981).
[16] D. Baye and P. H. Heenen, J. Phys. A **19**, 2041 (1986).
[17] D. Baye *et al.*, J. Phys. B **31**, 3439 (1998).
[18] B. C. Eu and J. Ross, J. Chem. Phys. **44**, 2467 (1966).
[19] E. J. Heller, Chem. Phys. Lett. **23**, 102 (1973).
[20] R. Der, O. Gebhardt, and R. Haberlandt, Chem. Phys. Lett. **27**, 107 (1974).
[21] J. Gerratt, Phys. Rev. A **30**, 1643 (1984).
[22] C. J. Bocchetta and J. Gerratt, J. Chem. Phys. **82**, 1351 (1985).
[23] N. F. Lane, Rev. Mod. Phys. **52**, 29 (1980).
[24] M. LeDourneuf, B. I. Schneider, and P. G. Burke, J. Phys. B **12**, L365 (1979).
[25] B. K. Sarpal, J. Tennyson, and L. A. Morgan, J. Phys. B **27**, 5943 (1994).
[26] J. D. Gorfinkiel *et al.*, Eur. Phys. J. D **35**, 231 (2005).
[27] M. Hori *et al.*, Phys. Rev. Lett. **94**, 063401 (2005).
[28] I. Shimamura, Phys. Rev. A **46**, 3776 (1992).
[29] A. I. Florescu-Mitchell and J. B. A. Mitchell, Phys. Rep. **430**, 277 (2006).
[30] M. E. Rose, *Elementary Theory of Angular Momentum* (Wiley, New York, 1957).
[31] M. J. Seaton, Comput. Phys. Commun. **146**, 225 (2002).
[32] E. B. Wilson and J. B. Howard, J. Chem. Phys. **4**, 260 (1936).
[33] K. Sakimoto, Phys. Rev. A **65**, 012706 (2001).
[34] C. Bloch, Nucl. Phys. **4**, 503 (1957).
[35] E. S. Chang and U. Fano, Phys. Rev. **6**, 173 (1972).
[36] J. Dubau, J. Phys. B **11**, 4095 (1978).
[37] E. B. Stechel, R. B. Walker, and J. C. Light, J. Chem. Phys. **69**, 3518 (1978).
[38] K. L. Baluja, P. G. Burke, and L. A. Morgan, Comput. Phys. Commun. **27**, 299 (1982).
[39] K. A. Berrington *et al.*, J. Phys. B **20**, 6379 (1987).
[40] E. G. Layton, J. Phys. B **26**, 2501 (1993).
[41] L. Malegat, J. Phys. B **27**, L691 (1994).
[42] M. Plummer and C. J. Noble, J. Phys. B **32**, L345 (1999).
[43] L. A. Morgan, Comput. Phys. Commun. **31**, 419 (1984).
[44] M. Abramowitz and I. E. Stegun, *Handbook of Mathematical Functions*, Natl. Bur. Stand. Appl. Math. Ser. 55 (U.S. GPO, Washington, DC, 1964), Chap. 22.
[45] K. Sakimoto, J. Chem. Phys. **112**, 5044 (2000).
[46] P. J. A. Buttle, Phys. Rev. **160**, 719 (1967).
[47] U. Fano, J. Opt. Soc. Am. **65**, 979 (1975).
[48] M. J. Seaton, Rep. Prog. Phys. **46**, 167 (1983).
[49] R. J. Whitehead, J. F. McCann, and I. Shimamura, Phys. Rev. A **64**, 023401 (2001).
[50] X. M. Tong, K. Hino, and N. Toshima, Phys. Rev. Lett. **97**, 243202 (2006).
[51] J. S. Cohen, Phys. Rev. A **69**, 022501 (2004).
[52] N. Chandra and A. Temkin, Phys. Rev. A **13**, 188 (1976).
[53] K. Sakimoto, Phys. Rev. A **66**, 032506 (2002).
[54] E. Fermi and E. Teller, Phys. Rev. **72**, 399 (1947).
[55] W. R. Garrett, Phys. Rev. A **3**, 961 (1971).
[56] I. Shimamura, Phys. Rev. A **40**, 4863 (1989).